

FEDSM-ICNMM2010-30770

COOLING IN CONSTANT WALL TEMPERATURE MICROCHANNELS WITH THERMAL CREEP EFFECTS

Ali Amiri-Jaghargh

Ferdowsi University of Mashhad
Mechanical Engineering Department
Mashhad, Iran

Hamid Niazmand

Ferdowsi University of Mashhad
Mechanical Engineering Department
Mashhad, Iran

Metin Renksizbulut

University of Waterloo
Mechanical & Mechatronics Engineering Department
Waterloo, Ontario, Canada

ABSTRACT

Fluid flow and heat transfer in the entrance region of rectangular microchannels of various aspect ratios, $0.2 \leq \alpha^* \leq 1$, are numerically investigated in the slip flow regime, $10^{-3} \leq Kn \leq 10^{-1}$, with particular attention to the thermal creep effects. Uniform inlet velocity and temperature profiles are prescribed in a microchannel with constant wall temperature. The gas inlet temperature is prescribed higher than the wall temperature in order to study the thermal creep effects in a fluid cooling process. To avoid unrealistically large axial temperature gradients due to the prescribed uniform inlet temperature and upstream conduction associated with low Reynolds number flows encountered in microchannels, an adiabatic section is added to the inlet of the channel, which resembles an adiabatic reservoir. A control volume technique is employed to solve the Navier-Stokes and energy equations which are accompanied with appropriate velocity-slip and temperature-jump boundary conditions at walls. Despite the constant wall temperature, axial and peripheral temperature gradients form in the gas layer adjacent to the wall due to temperature-jump. The simultaneous effects of velocity-slip, temperature-jump and thermal creep on the flow and thermal patterns along with the key flow parameters are examined in detail for a wide range of cross sectional aspect ratios, and Knudsen and Reynolds numbers ($0.1 \leq Re \leq 5$). Present results indicate that thermal creep effects influence the flow field and the temperature distribution significantly in the early section of the channel.

INTRODUCTION

In recent years, fluid flow and heat transfer at micro scales have gained much significance due to rapid progress made in the miniaturization of practical engineering devices such as heat exchangers and chemical reactors. Some of these applications involve rarefied gas flows in rectangular microchannels. Although gas flows in microchannels can occur in different flow regimes, the slip flow regime is more commonly encountered. In micro scale devices, the characteristic dimensions may be comparable to the mean free path of the molecules, and therefore, the gas flow is associated with some degree of rarefaction even in relatively high pressure applications. The Knudsen number, which is defined as the ratio of the molecular mean free path to the appropriate length scale of the device is a proper parameter to measure this effect. Flow with Knudsen number in the range of $10^{-3} \leq Kn \leq 10^{-1}$, relevant to most microchannel applications, is called slip-flow. In this regime, a departure from local thermodynamic equilibrium occurs in a thin layer adjacent to the wall, called Knudsen layer, so that the classical continuum assumption begins to fail. However, much theoretical and experimental evidence [1-3] support the continued use of the standard Navier-Stokes equations provided that they are accompanied by modified boundary conditions, which are known as the velocity-slip and temperature-jump conditions. Based on momentum and energy balances near a surface, it can be shown that the velocity slip and temperature jump are proportional to their normal gradients at the wall.

In applications where considerable tangential temperature gradients exist, another contribution to velocity slip emerges known as thermal creep. It must be noted that axial temperature gradients can form in the gas layer adjacent to the walls even along a constant-wall-temperature microchannel due to the temperature jump condition. In the absence of other driving forces, thermal creep generates a flow surprisingly from cold to hot. Therefore, it plays different roles depending on the positive or negative sign of the existing axial temperature gradient. In a fluid heating process, thermal creep effects reinforce the slip velocity contribution from the normal velocity gradient, while in a fluid cooling process, thermal creep opposes the flow.

A survey of the available literatures reveals a limited number of studies on the effects of thermal creep in microchannels. The temperature driven micro flows in both planar and cylindrical tubes in transitional flow regime were numerically studied by Alexeenko et al. [4] using DSMC (Direct Simulation Monte Carlo) method. They applied different wall temperature distributions to study thermal creep effects in a Knudsen compressor. Zhu et al. [5] developed a theoretical analysis based on orthogonal functions to study gaseous flow in arbitrary shape microchannels considering thermal creep effects. They found that thermal creep flow decreases friction coefficient when the microchannel is heated. Simultaneously developing slip flow with prescribed constant creep velocities in the entrance region of a planar microchannel was numerically investigated by Rig et al. [6]. They also presented an analytical solution for fully developed flow, and have recently [7] extended their studies to rectangular microchannels. It is concluded that thermal creep causes an increase in friction coefficient for cooling case while it has an opposing effect in heating. The effects of thermal creep on natural convection in a vertical isothermal microchannel were numerically studied by Chen and Weng [8]. It was found that thermal creep increases the flow rates, reduces friction, and enhances heat transfer. In their more recent study [9], a constant-wall-heat-flux microchannel was considered and similar findings were reported.

Sazhin et al. [10] studied the thermal creep phenomenon through straight cylindrical capillaries in the free molecular flow regime using the DSMC method. Méolans and Graur [11] developed an analytical model for thermal creep flow. They considered a planar microchannel between two reservoirs maintained at the same pressure, while a constant temperature gradient was applied along the channel. Bao and Lin [12] used the Burnett equations with slip boundary conditions to model compressible gas flow and heat transfer in micro Poiseuille flow in the slip and transition-flow regimes. The thermal creep contribution on the slip velocity was taken into consideration in the simulation. They concluded that thermal creep only affects the velocity slip in the entrance region, where high tangential temperature gradients occur. Using a perturbation method, an analytical solution for the velocity field in compressible Poiseuille flow with a constant heat flux boundary condition was derived by Ghahremani et al. [13]. They concluded that thermal creep increases the velocity and the flow rate for a heating case. It was also shown that this effect is only considerable for low orders of magnitude of the Brinkman number (as low as 10^{-2}).

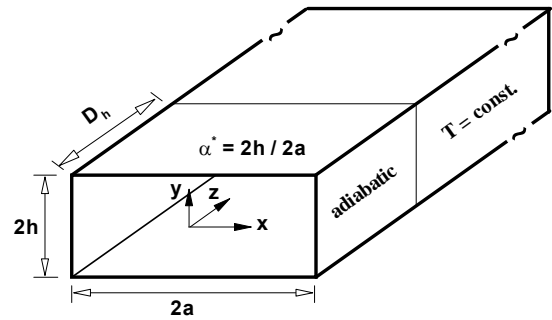


FIGURE 1. FLOW GEOMETRY AND COORDINATES.

This brief review reveals that analytical studies related to the effects of thermal creep are usually restricted to the fully developed conditions and simplified geometries, while in numerical calculations thermal creep has been studied either assuming a constant temperature gradient at the walls or a prescribed creep velocity. Furthermore, none of the available literature is focused on the details of thermal creep as a contributor of velocity slip. Therefore, there is a need for further studies to identify the thermal creep effects especially in cases where these simplifying assumptions are not employed.

In the present study, incompressible gaseous slip-flows and heat transfer in the entrance region of rectangular microchannels are investigated. The inlet temperature of the gas is assumed to be higher than the constant wall temperature to simulate a cooling condition. Three-dimensional Navier-Stokes and energy equations along with velocity-slip and temperature-jump boundary conditions are solved numerically by a control-volume method. The effects of thermal creep and axial heat conduction are included in the analysis. Flow fields, temperature distributions and, friction and heat transfer coefficients are examined in detail for a wide range of Reynolds numbers, $0.1 \leq Re \leq 5$, aspect ratios, $0.2 \leq \alpha^* \leq 1$, and Knudsen numbers, $Kn \leq 0.1$.

MATHEMATICAL MODEL

Figure 1 shows the flow geometry and the coordinate system. An important issue associated with low Reynolds number flows is the fact that axial heat conduction in the upstream direction can affect the inlet temperature profile significantly, thereby creating an inconsistency with a specified constant-temperature inlet boundary condition. Numerically enforcing such a condition leads to unrealistic axial temperature gradients in the gas layer adjacent to the wall at the inlet, where the inlet temperature abruptly changes to the wall temperature. To avoid this problem, an adiabatic section has been added to the channel inlet, which has a length of one hydraulic diameter. Thereafter, the constant wall temperature is applied.

The governing parameters related to the microchannel flows are the Reynolds and Knudsen numbers which are defined as $Re = \rho w_i D_h / \mu$ and $Kn = \lambda / D_h$ where w_i , D_h and λ are the inlet velocity, hydraulic diameter and molecular mean free path, respectively. The mean free path is evaluated based on the inlet conditions according to:

$$\lambda = \frac{\mu}{\rho\sqrt{2RT/\pi}} \quad (1)$$

where R is the specific gas constant taken as $R = 287 \text{ J/kg.K}$ for all cases considered here. For a given Knudsen number the hydraulic diameter is calculated from $D_h = \lambda / \text{Kn}$, and the channel dimensions are then fixed based on the given channel aspect ratio, $a^* = 2h / 2a$, and the definition of the hydraulic diameter, $D_h = 4(ah) / (a+h)$.

Laminar flow is considered with negligible compressibility effects in the limit of low Mach number flows. Assuming constant thermophysical properties, the governing equations including continuity, momentum and energy conservation are as follows:

$$\int_A \rho \vec{V} \cdot d\vec{A} = 0 \quad (2)$$

$$\frac{\partial}{\partial t} \int_V \rho \vec{V} dV + \int_V \rho \vec{V} \cdot \nabla \vec{V} dV = - \int_A p d\vec{A} + \int_A \mu \nabla \vec{V} \cdot d\vec{A} \quad (3)$$

$$\frac{\partial}{\partial t} \int_V \rho c_p T dV + \int_V \rho c_p \vec{V} \cdot \nabla T dV = \int_A k \nabla T \cdot d\vec{A} \quad (4)$$

where \vec{V} , T , ρ , p , μ , c_p and k are the velocity vector, temperature, density, pressure, dynamic viscosity, specific heat and thermal conductivity, respectively. The convective terms in the momentum and energy equations are transformed into volume integrals (non-conservative form) in order to limit the errors that can propagate due to the sensitivity of the continuity equation in low Mach number flows.

Boundary Conditions

Inflow boundary conditions correspond to uniform flat profiles such that $w = w_i = w_m$ and $T = T_i$ where subscripts i and m refer to inlet and mean bulk condition, respectively. The inlet velocity is obtained from Reynolds number while the inlet temperature $T_i = 350\text{K}$ is applied in all cases. Fully developed conditions with zero gradients are assumed at the outlet, while the pressure is set to zero. At all other boundaries including the inlet, zero pressure gradients are applied. It is verified that an axial length of $5D_h$ is required for fully developed conditions to be established. The flow satisfies the well known first order velocity-slip and temperature-jump boundary conditions at the walls as:

$$w_s = \left(\frac{2 - \sigma_v}{\sigma_v} \right) \lambda \left(\frac{\partial w}{\partial n} \right)_g + \frac{3}{4} \frac{\mu}{\rho T_g} \left(\frac{\partial T}{\partial s} \right)_g \quad (5)$$

$$T_g - T_w = \left(\frac{2 - \sigma_T}{\sigma_T} \right) \left(\frac{2\gamma}{\gamma + 1} \right) \frac{\lambda}{\text{Pr}} \left(\frac{\partial T}{\partial n} \right)_g \quad (6)$$

The other velocity components are specified similarly. Here, w_s is the slip velocity defined as $w_s = w_g - w_w$ which is the difference between wall velocity, w_w , and velocity of the gas adjacent to the wall, w_g . The subscript w identifies a wall with a normal coordinate n and tangential coordinate s . The subscript g indicates the first layer of the gas adjacent to the

wall where the normal and tangential gradients are evaluated. The coefficients σ_v and σ_T , known as the tangential-momentum and energy accommodation coefficients, are usually determined experimentally. For many engineering applications they are close to one and are taken as unity for simplicity. The last term in Eqn. (5) is known as thermal creep, which implies that tangential temperature gradients at a wall can introduce fluid flow in the absence of any other deriving force in the direction from cold to hot. The wall temperature and Prandtl number are set equal to $T_w = 300\text{K}$ and $\text{Pr} = 1$, respectively, for all cases considered in the present work.

NUMERICAL MODEL

The numerical solution is based on a projection-type method which solves the flow field in two steps. First, an intermediate velocity field is obtained using the available pressure field. Next, velocity and pressure corrections are calculated from a Poisson equation designed to satisfy the continuity equation. The numerical scheme was originally developed by Chorin [14], and improved further by Dwyer [15] and Niazmand et al. [16]. Also, a pressure correction based on the conservation of cross sectional mass flux is introduced, which greatly enhances the convergence rate of the numerical scheme. A pressure defect for a given cross section is associated with the average velocity defect $\Delta w'$ at the same cross section according to the following equation:

$$\rho \frac{\Delta w'}{\Delta t} = - \frac{\partial p'}{\partial z} \quad (7)$$

The average velocity defect is defined as $\Delta w' = \bar{w} - w_i$ where \bar{w} is the cross sectional averaged velocity. Thus, the pressure field is updated through the above correction and then the new velocity field is obtained using the updated pressure field.

The details of the grid independence studies, as well as evidence of accuracy in predicting the microchannel flow features are given elsewhere [18], and therefore, will not be repeated here. For most cases considered here a mesh of at least $51 \times 51 \times 141$ grid points in x , y and z directions with expansion ratios of 1.06, 1.1 and 1.015, respectively, has been used.

RESULTS AND DISCUSSION

As mentioned earlier, the Reynolds number is defined based on the inlet mean velocity and hydraulic diameter, $\text{Re} = \rho w_m D_h / \mu$. Since density is constant, for a given Reynolds number, the cross sectional mean inlet velocity can be calculated, which is also constant along the channel, $w_m = w_{in}$. Thermophysical properties of air at the inlet temperature have been used for all cases; however, the thermal conductivity has been adjusted such that a Prandtl number of one is preserved. The main advantage of $\text{Pr} = 1$ is the fact that the normalized axial length for both momentum and energy equations becomes identical corresponding to the same physical axial location which facilitates comparisons, $z^+ = z / (D_h \text{Re}) = z / (D_h \text{Pr Re}) = z^*$.

This study is restricted to low Reynolds number flows, $\text{Re} \leq 5$, associated with microchannel applications and in accordance with compressibility limitations which restrict the Reynolds number as the Knudsen number increases. Since in

the present study Pr is assumed as unity, low Re flows correspond to low Peclet number flows ($Pe = RePr$) in which axial conduction is large enough to affect the upstream temperature distribution, especially for $Pe < 1$ where axial conduction begins to dominate advection. In such cases, assuming a uniform temperature profile at the channel inlet is physically inappropriate because upstream conduction affects the inlet temperature profile. As mentioned earlier, this problem can be relaxed by considering a short adiabatic section at the channel inlet. It should be noted that for slip flows, the assumption of uniform inlet velocity profile is less problematic due to the relatively flat profiles that exist close to the inlet as a result of large velocity slip in the entrance region.

In the following sections, the effects of velocity-slip, temperature-jump and thermal creep on the velocity field and the temperature distribution will be discussed. Furthermore, slip effects on the friction and heat transfer coefficients will be examined in detail.

Velocity Field

Slip velocity at the walls leads to a flatter velocity profile and decreases the pressure gradient in comparison to no-slip cases for the same mass flux. Thermal creep as a contributor to velocity slip may enhance or weaken these effects depending on the sign of the axial temperature gradient in the first layer of the gas adjacent to the wall. It enhances the velocity slip in fluid heating cases, where a positive temperature gradient exist

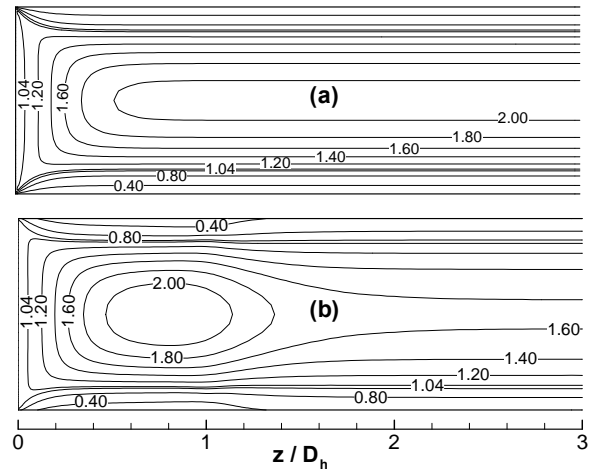


FIGURE 2. COMPARISON OF AXIAL VELOCITY FIELD AT $Re = 0.1$ FOR (a) $Kn = 0$ (b) $Kn = 0.1$

while it has opposing effects in the case of fluid cooling with negative axial temperature gradient. The axial velocity contours in the symmetry plane of a square microchannel at $Re = 0.1$ for both the no-slip ($Kn = 0$) and slip ($Kn = 0.1$) cases are shown in Figs. 2a and 2b, respectively. Velocity contours for the slip case indicate that the slip velocity is small in adiabatic section, where

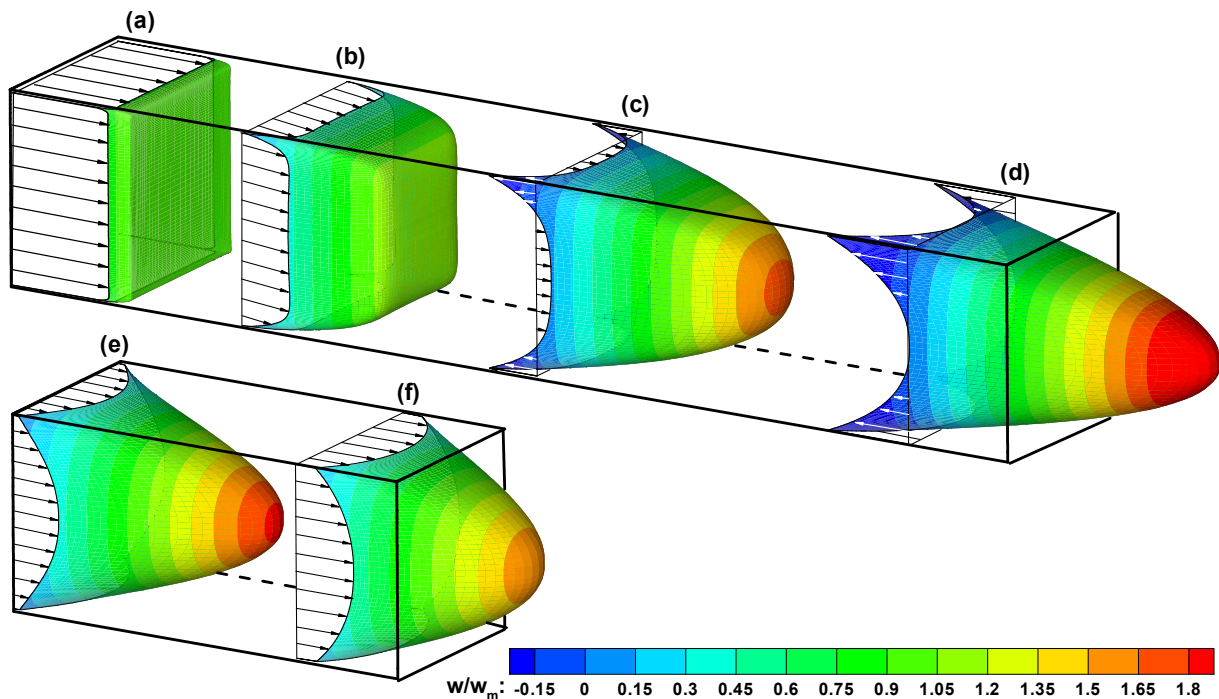


FIGURE 3. AXIAL VELOCITY PROFILE DEVELOPMENT ALONG A SQUARE CHANNEL FOR $Re = 0.1$ AND $Kn = 0.1$ AT SELECTED AXIAL LOCATIONS: $z^+ = z/(D_h Re) = 0.11, 1.02, 3.05, 7.85, 13.04$ AND 20.02 .

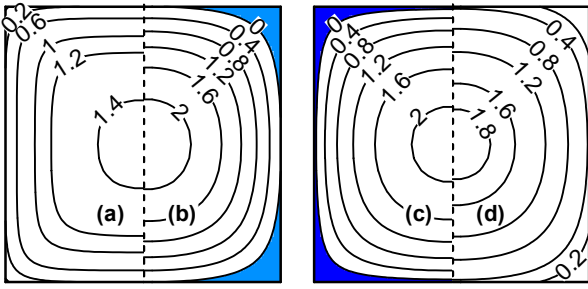


FIGURE 4. AXIAL VELOCITY CONTOURS ALONG A SQUARE CHANNEL, AND IDENTIFICATION OF REVERSE FLOW REGIONS, FOR $Kn = 0.1$ AT
(a) $z^+ = 2.05$, (b) $z^+ = 7.85$, (c) $z^+ = 10.0$, (d) $z^+ = 12.45$

thermal creep contribution is considerable, and the contours are to some extent similar to that of the no-slip case. However, as the flow leaves the adiabatic section, the effect of thermal creep diminishes and slip velocity increases gradually to a higher constant value in the fully developed region.

More details of the axial velocity profile variations along the channel are shown in Fig. 3, where three dimensional axial velocity profiles are plotted at some selected axial locations for the same flow conditions as those in Fig. 2b. Figure 3 shows that, at the very early sections of the channel, large velocity slip exist, while it rapidly ($z^+ > 2$) decreases due to the thermal creep effect. These effects in the adiabatic section are strong enough to form reverse flows in the corners where the normal velocity gradients are rather weak. The reverse flow regions are clearer in Fig. 4, where the axial velocity contours at different axial locations at $Kn = 0.1$ are shown. In this figure, the reverse flow regions are colored in blue and darker blue indicates stronger reverse flow. Due to the symmetry only half of the cross sections are plotted. The reverse flow appears after $z^+ = 2.05$ (Fig. 4-a), reaches its maximum around $z^+ = 10$, where maximum axial temperature gradients exist, and completely vanishes somewhere before $z^+ = 12.45$ (Fig. 4-d). Thermal creep effects vanish fairly fast in the constant wall temperature section and the velocity profiles become flatter due to the contribution of the normal gradient to slip velocity as shown in cross sections (e) and (f) in Fig. 3.

To identify the relative importance of the different contributions to the velocity slip, the axial variation of the peripherally-averaged velocity-slip normalized by the cross sectional averaged axial velocity, along with the contributions of the normal velocity gradients and axial temperature gradients are shown in Fig. 5 for a square microchannel at $Re = 0.1$ and $Kn = 0.1$. The thermal creep contribution is basically negative throughout the adiabatic section and it reaches its maximum negative value at the beginning of the constant wall temperature section, where the maximum axial temperature gradients occur. This negative contribution is responsible for the reverse flow described above.

However, in the constant temperature section, axial temperature gradients near the wall vanish rather fast, and consequently, the thermal creep effects disappear, while normal

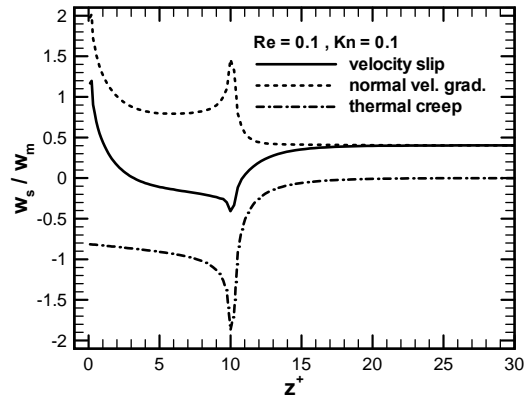
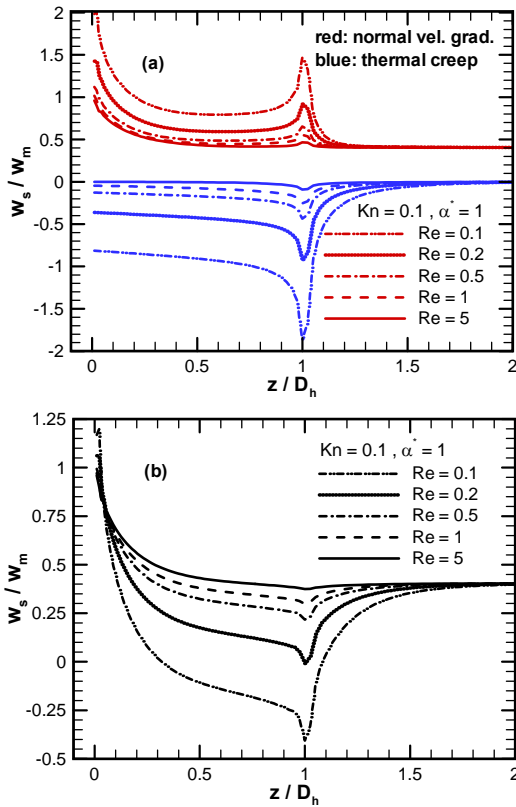


FIGURE 5. AXIAL VARIATIONS OF VELOCITY SLIP AND ITS COMPONENTS IN A SQUARE MICROCHANNEL AT $Re = 0.1$ AND $Kn = 0.1$.

velocity gradients assume a constant value in the fully developed region leading to a considerable cross sectional averaged velocity slip at the higher end of the slip-flow regime.

For a given geometry velocity slip is a function of Reynolds and Knudsen numbers. Clearly, larger Reynolds numbers increase the cross sectional averaged velocities leading to larger normal velocity gradients at the walls in the entrance region. At the same time, the upstream axial conduction decreases relative to the stronger stream wise convection, which reduces the axial temperature gradients in the adiabatic section. Therefore, it is to be expected that thermal creep effects become weaker at higher Reynolds numbers as shown in Figs. 6a-b. In these figures, the axial variations of the normalized peripherally-averaged slip components and total velocity-slip are plotted for $Kn = 0.1$ and different Reynolds numbers in a square microchannel. Basically, thermal creep effects in microchannel cooling flows can be safely ignored for Reynolds numbers higher than about 5. Also note that in the fully developed region, the slip velocity is almost independent of Reynolds number.

Since thermal creep effects are more pronounced at lower Reynolds numbers, Knudsen number effects on velocity slip are considered in Fig. 7 at $Re = 0.1$ for a square microchannel. Similar to Fig. 6, the axial variations of the normalized peripherally-averaged velocity slip are plotted. In this figure, thermal creep effects are shown separately in the lower right hand corner for more clarity. As indicated by Eqn. (5), the normal velocity gradient contribution to the velocity slip is directly related to Kn , and therefore, increases at higher Knudsen numbers. However, thermal creep effects are not directly influenced by the Knudsen number. Yet, since the velocity field is affected by slip due to the normal velocity gradients, which in turn affects the temperature field, thermal creep effects slightly increase with an increase in Knudsen number. Note that thermal creep dependence on Knudsen number is much weaker than the normal velocity gradient component. Therefore, as shown in Fig. 7, thermal creep effects are more pronounced at lower Knudsen numbers, where the normal velocity gradient contribution to slip is weaker.



FIGURES 6a-b. EFFECTS OF REYNOLDS NUMBER ON VELOCITY SLIP FOR A SQUARE MICROCHANNEL AT $Kn = 0.1$: (a) VELOCITY-SLIP COMPONENTS; (b) TOTAL VELOCITY-SLIP.

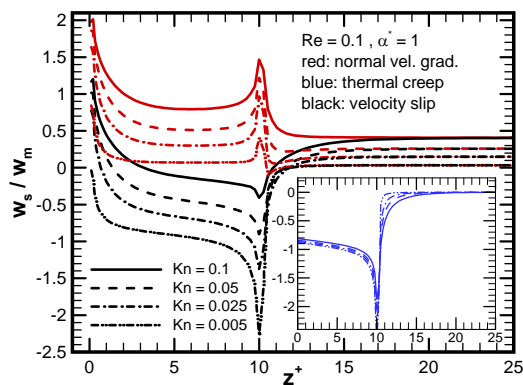


FIGURE 7. EFFECTS OF KN NUMBER ON VELOCITY SLIP AND ITS CONTRIBUTIONS FOR A SQUARE MICROCHANNEL AT $Re = 0.1$.

Velocity slip associated with microchannel flows in the slip flow regime reflects directly into the pressure drop, which is expressed in non-dimensional form in an apparent friction coefficient. Variations of the apparent friction coefficient in the entrance region of a square microchannel at $Re = 1$ for different

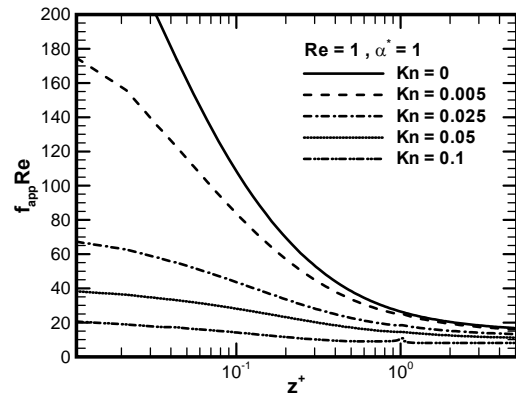


FIGURE 8. AXIAL VARIATIONS OF THE APPARENT FRICTION COEFFICIENT IN A SQUARE MICROCHANNEL AT $Re = 1$.

Knudsen numbers are shown in Fig. 8. The major reduction in the apparent friction coefficient at higher Knudsen numbers can be attributed to two factors. Slip reduces the wall shear stresses, and at the same time, less pressure drop is required for transforming the velocity profile from a uniform inlet profile to the fully developed profile, since the fully developed velocity profiles are much flatter as compared to those associated with no-slip flows.

As mentioned earlier, thermal creep effects are more pronounced at lower Reynolds numbers as shown in Fig. 9, where the axial variations of the apparent friction coefficient are shown for flow conditions similar to those in Fig. 8, except for the Reynolds number. Since thermal creep reduces the velocity slip in a cooling process, the flow experiences higher pressure drops. It is interesting that at the lower end of the slip-flow regime, thermal creep effects lead to pressure drops even higher than found in no-slip flows due to weaker normal velocity gradients. The local increase around the entrance to the constant wall temperature section is related to the high axial temperature gradients that exist there.

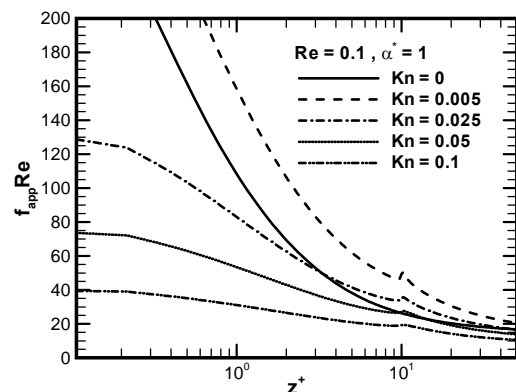


FIGURE 9. AXIAL VARIATIONS OF THE APPARENT FRICTION COEFFICIENT IN A SQUARE MICROCHANNEL AT $Re = 0.1$.

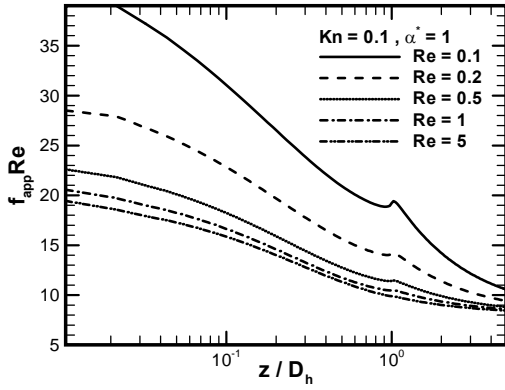


FIGURE 10. EFFECTS OF REYNOLDS NUMBER ON THE AXIAL VARIATIONS OF APPARENT FRICTION COEFFICIENTS IN A SQUARE MICROCHANNEL AT $Kn = 0.1$.

To elaborate more on the Reynolds number influence on pressure drop, the apparent friction factor in a square channel is plotted at $Kn = 0.1$ for several Reynolds numbers in Fig. 10. The apparent friction coefficient at the inlet, decreases by about 50% as Reynolds number increases from $Re = 0.1$ to $Re = 5$. Neglecting the spike at $z / D_h = 1$, which becomes weaker at higher Reynolds numbers, the friction coefficient decrease monotonically from finite values at the inlet to a single constant fully-developed value (fully-developed region is not included in this figure). The fact that the inlet friction coefficient is finite in the slip-flow regime has been acknowledged by other researchers as well [19, 20].

In the fully-developed region, the friction coefficient is only a function of the Knudsen number and the geometry of the channel. In Fig. 11, the fully-developed friction coefficients for several channel aspect ratios as a function of Knudsen number are plotted. Pressure drops associated with narrower channels

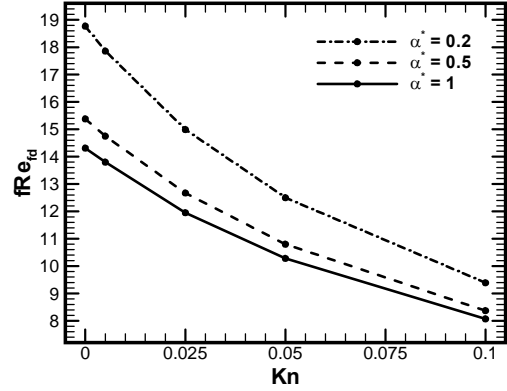


FIGURE 11. FULLY DEVELOPED FRICTION COEFFICIENTS AS A FUNCTION OF KNUDSEN NUMBER FOR MICROCHANNELS WITH DIFFERENT ASPECT RATIOS.

are higher, while velocity-slip, which increases at higher Knudsen numbers, decreases the friction coefficients dramatically, particularly at lower aspect ratios. For example, in a square microchannel, the fully developed friction coefficient at $Kn = 0.1$ is about 43% of that at $Kn = 0$. This reduction increases to about 50% for a channel with an aspect ratio of 0.2.

Temperature Field

The velocity and temperature fields are coupled due to the thermal creep component in the velocity slip boundary condition. Therefore, a simultaneous solution of the momentum and energy equations is required, which increases the computational effort. In a constant wall temperature flow, the nondimensional temperature can be defined as:

$$\theta = \frac{T - T_w}{T_i - T_w} \quad (8)$$

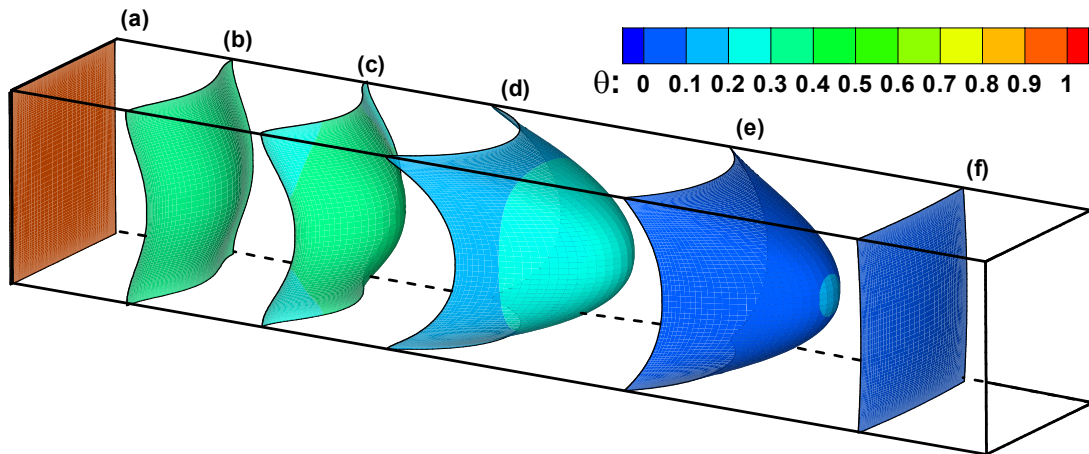


FIGURE 12. DEVELOPMENT OF THE TEMPERATURE PROFILE ALONG A SQUARE MICROCHANNEL AT $Re = 0.1$ AND $Kn = 0.1$: $z^+ = z/(D_h Re) = 0.11, 7.85, 8.77, 10, 13.04, 20.02$.

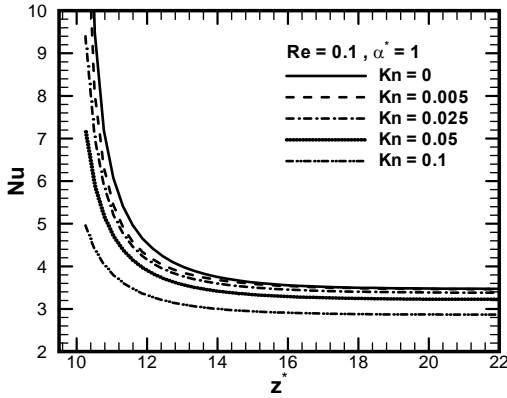


FIGURE 13. AXIAL VARIATIONS OF THE NUSSELT NUMBER IN A SQUARE MICROCHANNEL AT DIFFERENT Kn FOR $Re = 0.1$.

where T_i and T_w are the inlet and wall temperatures, respectively. The development of the temperature profiles from a uniform inlet profile to the wall temperature far from the inlet are shown in Fig. 12 for the same flow conditions as those in Fig. 3. Note that the temperature profiles are relatively flat along the channel and are stretched in Fig. 12 for more clarity.

The circumferentially-averaged local heat transfer coefficients along a square microchannel at $Re = 1$ are plotted in Fig. 13. As expected, the heat transfer coefficients decrease monotonically to their fully developed values along the channel. In general, temperature-jump acts like a contact resistance and is directly related to the Knudsen number. Therefore, at higher Knudsen numbers temperature-jump further reduces the heat transfer coefficients.

Unlike the fully-developed friction coefficients, which are independent of Reynolds number, at low Reynolds numbers, the heat transfer coefficients are influenced by the Reynolds number in the fully-developed region. The axial variations of Nusselt number along a square channel at $Kn = 0.1$ are shown in Fig. 14 for various Reynolds numbers.

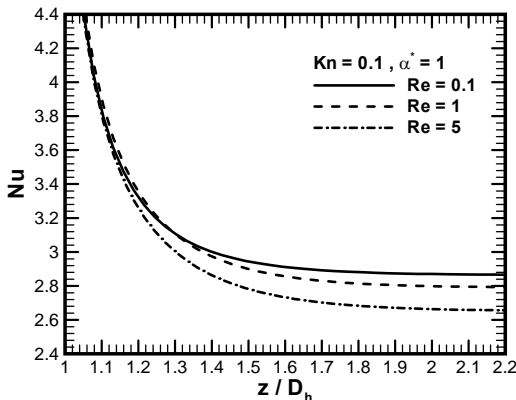


FIGURE 14. AXIAL VARIATIONS OF THE NUSSELT NUMBER IN A SQUARE MICROCHANNEL AT $Kn = 0.1$ AND DIFFERENT Re .

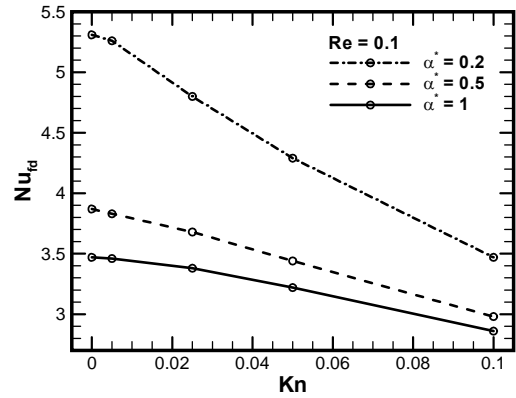


FIGURE 15. FULLY-DEVELOPED HEAT TRANSFER COEFFICIENTS AS A FUNCTION OF ASPECT RATIO FOR VARIOUS KNUDSEN NUMBERS.

As mentioned earlier, temperature-jump is more pronounced at higher Reynolds numbers due to larger normal temperature gradients, therefore, the heat transfer rates are expected to decrease as the Reynolds number increases. A reduction of about 8% in the fully-developed Nusselt number occurs as the Re increases from 0.1 to 5 at $Kn = 0.1$.

The fully-developed heat transfer coefficients are reduced in the slip-flow regime with an increase in Knudsen number as shown in Fig. 15, where the Nusselt number is plotted as a function of Knudsen number for $Re = 1$ and different aspect ratios. However, this reduction is not expected intuitively, since velocity slip tends to increase heat transfer due to enhanced advection effects, while temperature-jump acts like contact resistance and reduces the heat transfer rate. It seems the temperature jump effect is more dominant, and thus, the heat transfer rate decreases as the Knudsen number increases.

In general, in no-slip flows, as the aspect ratio decreases from a square channel towards the parallel plate limit, the heat transfer rates increase, since corner regions with weak temperature gradients become less dominant. Present results indicate a similar trend in the slip-flow regime, however, to some lower extent due to slip, which reduces the corner effects. For example, at $Re = 0.1$, as the aspect ratio increase from $\alpha^* = 0.2$ to $\alpha^* = 1$, the fully-developed Nusselt number decreases by about 35% in no-slip flow, while it decreases by about 18% for $Kn = 0.1$. It is interesting to note that in a rectangular microchannel with an aspect ratio of $\alpha^* = 0.2$, at the upper limit of the slip-flow regime, Nu is almost equal to that of a square microchannel in no-slip flow.

CONCLUSION

Rarefied gaseous flows in isothermal-wall rectangular microchannels of various aspect ratios, $0.2 \leq \alpha^* \leq 1$, have been numerically investigated in the continuum and slip-flow regimes, $Kn \leq 0.1$. Development of uniform inlet velocity and temperature profiles through the entrance region to their fully developed forms have been studied in a range of Reynolds numbers relevant to microchannel flows, $0.1 \leq Re \leq 5$. The flow is incompressible with constant properties and the Prandtl

number is set equal to one for all cases. The effects of velocity-slip and temperature-jump on the flow field and thermal patterns are examined in detail with particular attention to thermal creep effects. In a fluid heating process, thermal creep reinforces the slip velocity contribution arising from the normal velocity gradient, while in a fluid cooling process (studied in the present work), thermal creep opposes it.

It is found that the effects of thermal creep on velocity-slip are stronger at lower Reynolds numbers, where the normal velocity gradient contributions to velocity-slip are weaker. Furthermore, thermal creep effects are slightly affected by Knudsen number, while the normal gradient contribution is directly related to the Kn. Both friction and heat transfer coefficients decrease significantly due to rarefaction effects as Kn increases.

In contrast to the normal velocity gradient contribution to velocity-slip, which approaches a constant value in the fully developed region, thermal creep contribution mainly appears in the entrance region and vanishes in the fully-developed region. As a result, the fully-developed friction and heat transfer coefficients are basically the same for both processes of heating and cooling.

The fully-developed friction coefficient is only a function of geometry and Knudsen number, while the fully-developed heat transfer coefficient in low Reynolds number flows is related to the Reynolds number as well.

ACKNOWLEDGMENT

The financial support of the Natural Sciences and Engineering Research Council of Canada (NSERC) and the Ferdowsi University of Mashhad are gratefully acknowledged.

REFERENCES

- [1] Wu, P. and Little, W.A., 1983. "Measurements of friction factors for the flow of gases in very fine channels used for micro miniature Joule-Thomson refrigerators". *Cryogenics*, Vol. 23, pp. 273-277.
- [2] Beskok, A. and Karniadakis, G.E., 1992. "Simulation of slip-flows in complex micro geometries". *J. Micromech. Syst. DSC*, Vol. 40, pp. 355-370.
- [3] Turner, S.E., Lam, L.C., Faghri, M. and Gregory, O.J., 2004. "Experimental investigation of gas flow in microchannels". *J. Heat Transfer*, Vol. 126, pp. 753-763.
- [4] Alexeenko, A.A., Gimelshein, S.F., Phillip Muntz, E. and Ketsdever, A.D., 2006. "Kinetic modeling of temperature driven flows in short microchannels". *Int. J. Thermal Sciences*, Vol. 45, pp. 1045-1051.
- [5] Zhu, X., Liao, Q. and Xin, M.D., 2006. "Gas flow in microchannel of arbitrary shape in slip flow regime". *Microscale thermophysical engineering*, Vol. 10 (1), pp. 41-54.
- [6] Rij, J.V., Harman, T. and Ameel, T., 2007. "The effect of creep flow on two-dimensional isoflux microchannels". *Int. J. Thermal Sciences*, Vol. 46, pp. 1095-1103.
- [7] Rij, J.V., Ameel, T. and Harman, T., 2009. "An evaluation of secondary effects on microchannel frictional and convective heat transfer characteristics". *Int. J. Heat and Mass Transfer*, Vol. 52, pp. 2792-2801.
- [8] Chen, C. and Weng, H.C., 2006. "Developing natural convection with thermal creep in a vertical microchannel". *J. Phys. D: Appl. Phys.*, Vol. 39, pp. 3107-3118.
- [9] Weng, H.C. and Chen, C., 2008. "On the importance of thermal creep in natural convective gas microflow with wall heat fluxes". *J. Phys. D: Appl. Phys.*, Vol. 41, pp. 115501-115510.
- [10] Sazhin, O., Kulev, A., Borisov, S. and Gimelshein, S., 2008. "Numerical analysis of gas-surface scattering effect on thermal transpiration in the free molecular regime". *Vacuum*, Vol. 82, pp. 20-29.
- [11] Méolans, J.G. and Graur, I.A., 2008. "Continuum analytical modeling of thermal creep". *European Journal of Mechanics - B/Fluids*, Vol. 27, pp. 785-809.
- [12] Bao, F. and Lin, J., 2008. "Burnett simulation of gas flow and heat transfer in micro Poiseuille flow". *Int. J. Heat and Mass Transfer*, Vol. 51, pp. 4139-4144.
- [13] Ghahremani, A.R., Safari Mohsenabad, S. and Behshad Shafii, M., 2008. "Analytical Solution for Compressible Gas Flow Inside a Two-Dimensional Poiseuille Flow in Microchannels with Constant Heat Flux Including the Creeping Effect". *Proceedings of World Academy of Science, Engineering and Technology*, Vol. 33, pp. 2070-3740.
- [14] Chorin, A.J., 1968. "Numerical solution of the Navier-Stokes equations". *Math. Comput.*, Vol 22, pp. 745-762.
- [15] Dwyer, H.A., 1989. "Calculation of droplet dynamics in high temperature environments". *Prog. Energy Combust. Sci.*, Vol. 15, pp. 131-158.
- [16] Niazmand, H., Renksizbulut, M. and Saeedi, E., 2008. "Developing slip-flow and heat transfer in trapezoidal microchannels". *Int. J. Heat and Mass Transfer*, Vol. 51, pp. 6126-6135.
- [17] Renksizbulut, M. and Niazmand, H., 2006. "Laminar flow and heat transfer in the entrance region of trapezoidal channels with constant wall temperature". *J. Heat Transfer*, Vol. 128, pp. 63-74.
- [18] Niazmand, H., Amiri Jaghargh, A. and Renksizbulut, M., 2010. "Slip-flow and heat transfer in isoflux rectangular microchannels with thermal creep effect". *Journal of Applied Fluid Mechanics*, Vol. 3 (2), pp. 33-41.
- [19] Morini, G.L., M. Spiga and Tartarini, P., 2004. "The rarefaction effect on the friction factor of gas flow in microchannels". *Superlattices and Microstructures*, Vol. 35, pp. 587-599.
- [20] Hettiarachchi, H.D.M., Golubovic, M, Worek, W.M. and Minkowycz, W.J., 2008. "Three-dimensional laminar slip-flow and heat transfer in a rectangular microchannel with constant wall temperature". *Int. J. Heat and Mass Transfer*, Vol. 51, pp. 5088-5096.